

pubs.acs.org/accounts Article

Nonequilibrium Scattering/Evaporation Dynamics at the Gas-Liquid Interface: Wetted Wheels, Self-Assembled Monolayers, and Liquid Microjets

Published as part of the Accounts of Chemical Research special issue "Applications of Liquid Microjets in Chemistry".

David J. Nesbitt,* Alex M. Zolot, Joseph R. Roscioli, and Mikhail Ryazanov



Cite This: https://doi.org/10.1021/acs.accounts.2c00823

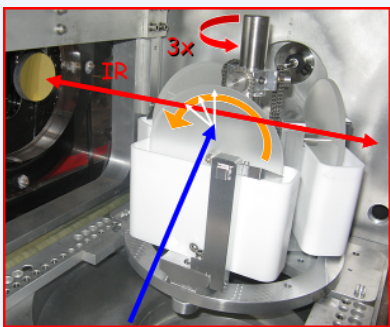


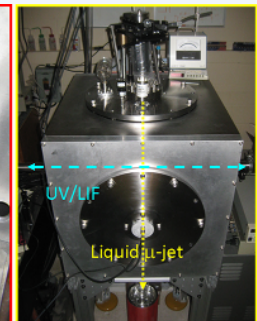
ACCESS

III Metrics & More

Article Recommendations

CONSPECTUS: We often teach or are taught in our freshman courses that there are three phases of matter—gas, liquid and solid—where the ordering reflects increasing complexity and strength of interaction between the molecular constituents. But arguably there is also a fascinating additional "phase" of matter associated with the microscopically thin interface (<10 molecules thick) between the gas and liquid, which is still poorly understood and yet plays a crucial role in fields ranging from chemistry of the marine boundary layer and atmospheric chemistry of aerosols to the passage of O₂ and CO₂ through alveolar sacs in our lungs. The work in this Account provides insights into three challenging new directions for the field, each embracing a rovibronically quantum-





state-resolved perspective. Specifically, we exploit the powerful tools of chemical physics and laser spectroscopy to pose two fundamental questions. (i) At the microscopic level, do molecules in all internal quantum-states (e.g., vibrational, rotational, electronic) colliding with the interface "stick" with unit probability? (ii) Can reactive, scattering, and/or evaporating molecules at the gas—liquid interface avoid collisions with other species and thereby be observed in a truly "nascent" collision-free distribution of internal degrees of freedom? To help address these questions, we present studies in three different areas: (i) reactive scattering dynamics of F atoms with wetted-wheel gas—liquid interfaces, (ii) inelastic scattering of HCl from self-assembled monolayers (SAMs) via resonance-enhanced photoionization (REMPI)/velocity map imaging (VMI) methods, and (iii) quantum-state-resolved evaporation dynamics of NO at the gas—water interface. As a recurring theme, we find that molecular projectiles reactively, inelastically, or evaporatively scatter from the gas—liquid interface into internal quantum-state distributions substantially out of equilibrium with respect to the bulk liquid temperatures (T_s). By detailed balance considerations, the data unambiguously indicate that even simple molecules exhibit rovibronic state dependences to how they "stick" to and eventually solvate into the gas—liquid interface. Such results serve to underscore the importance of quantum mechanics and nonequilibrium thermodynamics in energy transfer and chemical reactions at the gas—liquid interface. This nonequilibrium behavior may well make this rapidly emergent field of chemical dynamics at gas—liquid interfaces more complicated but even more interesting targets for further experimental/theoretical exploration.

■ KEY REFERENCES

- Hoffman, C. H.; Nesbitt, D. J. Quantum-state-resolved 3D velocity map imaging of surface-scattered molecules: Incident energy effects in HCl + self-assembled monolayer collisions. J. Phys. Chem. C 2016, 120, 16687–16698.¹ This work lays the foundation for REMPI/VMI study of quantum-state-resolved scattering from liquid mimetic SAM surfaces.
- Zolot, A. M.; Harper, W. W.; Perkins, B. G.; Dagdigian, P. J.; Nesbitt, D. J. Quantum-state-resolved reaction dynamics at the gas-liquid interface: Direct absorption

detection of HF(v,J) product from F(²P) plus squalane. J. Chem. Phys. **2006**, 125, 021101.² This work presents the first quantum-state-resolved IR results on reactive scattering of F atoms at the gas—hydrocarbon liquid interface,

Received: December 16, 2022



- providing evidence for highly nonequilibrium deposition of reaction exothermicity into rovibrational HF(v,J) products.
- Ryazanov, M.; Nesbitt, D. J. Quantum-state-resolved studies of aqueous evaporation dynamics: NO ejection from a liquid water microjet. J. Chem. Phys. 2019, 150, 044201.³ This is our first study on evaporation dynamics from liquid water, which provides clear evidence for postevaporative collisions of NO with H₂O adiabatically expanding from the gas-microjet interface.
- Livingston Large, T. A.; Nesbitt, D. J. Low energy CO scattering at the gas-liquid interface: Experimental/theoretical evidence for a novel sub-thermal impulsive scattering (STIS) channel. J. Phys. Chem. C 2020, 124, 28006–28017. This work with a wetted-wheel technique illustrates how IR laser absorption methods can be used to probe nonequilibrium internal quantum-state distributions for CO scattering from simple low vapor pressure liquids.

I. INTRODUCTION

The gas—liquid interface represents an extremely complex and challenging environment for investigation with modern chemical-physics methods, though one of critical relevance to molecular adsorption and chemical reaction phenomena from atmospheric droplets to the marine boundary layer. Collisions at the gas—liquid interface are crucial to a predictive understanding of chemical pathways ranging from adsorption, accommodation, and solvation of gases into liquids to heterogeneous gas—liquid-phase catalysis and reactive processing of molecular surfactants on atmospheric aerosols. $^{5-7}$ Indeed, in even more intimately human terms, such collisional processes are fundamental to molecular $\rm O_2$ adsorption into (and $\rm CO_2$ expulsion out of) our bloodstream through the lung alveoli, a respiration process obviously responsible for survival of the species. 8

The first step along this diverse and intricate dynamical pathway is through collisional energy transfer at the gas—liquid interface, which can be probed by molecular-beam experiments exploring the exchange of energy into the projectile's translational, rotational, vibrational, and electronic degrees of freedom. Pathonic his is an area with research advances spanning several decades, it is still a quite young, exciting, and rapidly evolving scientific field! Indeed, it represents a frontier discipline distinguished by early development of molecular-beam experiments by Fenn and co-workers and considerably advanced by Nathanson, Minton, and others, based on inelastic collisions of supersonic beams with liquid interfaces, monitored by time-of-flight mass spectrometry on the scattered atomic and molecular species. Pathonic mass spectrometry on the scattered atomic and molecular species.

Of particular interest have been prospects of controlled chemistry at the gas—liquid interface. The Nathanson group has been a vigorous leader in this area, utilizing time-of-flight mass spectrometry for probing redox reactions and H/D exchange processes for projectiles colliding with the gas—liquid interface. The Minton group has specialized in clever CO_2 "laser detonation" sources to achieve high fluxes of hyperthermal atomic/molecular projectiles $(O_2, O(^3P), O(^1D),$ etc.) with multiple-electronvolt translational energies, which has enabled many mass-spectroscopic studies of translationally hyperthermal reaction dynamics at both gas—liquid and gas—solid interfaces. 12,15,17,18 The Nesbitt group has taken advantage of high-resolution lasers and discharge-energized molecular beam sources to inelastically and/or reactively

scatter molecules and atomic radicals from a variety of liquid surfaces, providing detailed spectroscopic information on quantum-state and translational distributions of the scattered molecules by direct IR-laser absorption and Dopplerimetry. 19-23 The McKendrick group has elegantly applied quantum-state-resolved techniques with UV photolysis sources of translationally hot OH and O(3P) colliding with hydrocarbon and room-temperature ionic liquids (RTILs), probing the resulting rovibrational distributions of OH(v, N) by laserinduced fluorescence (LIF). 11,18,24-26 The net result of all these and many other studies has been deep mechanistic insights into chemical and physical properties of the gas-liquid interface. Crucially relevant to this collective body of work has been the use of rotating "wetted wheels" for generating gasliquid interfaces, with low vapor pressure fluids to maintain suitably high vacuum conditions. In particular, section II of this Account features one example of many such wetted-wheel studies from our group, 20,21,23,27 specifically utilizing ultrasensitive high resolution IR absorption spectroscopy for probing the nascent distributions of HF(v,J) emerging from H atom abstraction reactions by atomic beams of F radicals at the vacuum-squalane interface. 2,22

One persistent limitation to the implementation of such wetted-wheel methods, particularly for quantum-state-resolved studies, has been the requirement for low vapor pressure liquids to permit molecules to impinge on and escape from the gas-liquid interface without collisional scrambling. A powerful alternative approach to the wetted-wheel concept that circumvents most of these vapor pressure limitations involves the use of solution phase chemistry to form self-assembled monolayers (SAMs) of long chain organic thiols (R-SH) on nanometer thin Au coated surfaces. This platform has been extensively used in conjunction with molecular beam methods by Morris and co-workers²⁸ to study inelastic energy transfer at the gas-SAM interface via time-of-flight mass spectroscopy. The elegance of such methods is that the resulting monolayer self-adheres via weak van der Waals forces and therefore presents a "liquid-like" mimetic surface in vacuo to the incoming molecular beam. Furthermore, one can arbitrarily modify such long chain organic thiols with specific functional groups (alcohols, aldehydes, carboxylic acids, amines, etc.) and thereby "tune" the chemistry of the molecular "canopy" struck by the incoming beam. We have found it particularly powerful to combine these studies with 1 + 1 resonance-enhanced multiphoton ionization (REMPI) methods for selectively probing molecular projectiles in a single rovibrational quantum-state, which in conjunction with velocity map imaging (VMI) methods provides full 3D information on the scattered vector momenta. 29,30 In section III, we present examples involving such quantum-state-resolved scattering of supersonically cooled HCl(v = 0, J = 0) from alkyl-thiolated SAM surfaces under high-vacuum, single-collision conditions.¹

Although the use of SAMs offers a powerfully strategic alternative to low vapor pressure liquids for such interfacial dynamical studies, this does not avoid the simple fact that the most important liquid in nature (i.e., water) has a 20 Torr vapor pressure at room temperature! Such high vapor pressure 31 seriously limits gas—surface scattering studies with millimeter-scale laser probe beams, since typical mean free paths (λ_0) in the vapor phase are only a few micrometers. Thus, in terms of spin—orbit, electronic, vibrational, rotational, and translation degrees of freedom, the "nascent" distribution of any scattered/evaporating molecules can be rapidly

compromised by collisions prior to measurement. A clever technique to circumvent this problem, first demonstrated by Faubel, Schlemmer, and Toennies,³² has been to generate the gas-liquid water interface in the form of a "microjet", i.e., a flowing liquid column with a micrometer-scale radius (r_0) on the order of the gas-phase mean free path (λ_0) at equilibrium vapor densities. For a cylindrical geometry, the vapor density drops off as r_0/r from the jet axis; thus, although densities in the immediate proximity of the jet are similar to that of a flat water surface, they drop to much lower values within a few characteristic r_0 lengths. In principle, this seems an ideal "free lunch" for gas-liquid experimentalists: for small microjet diameters, the average number of collisions in the macroscopic distance between liquid surface and laser detection region can in principle be made negligible. In the final section of this work (section IV), we present sample studies from our laboratory on quantum-state-resolved NO evaporation from liquid water microjets, which both provide tantalizing evidence for nonequilibrium behavior and also highlight the very real experimental challenges in achieving such collision free conditions.³ What binds these three studies into a common theme is that quantum-state scattering distributions in each case signal the presence of nonequilibrium dynamics, which from detailed balance consideration necessarily implies a quantum-state dependence to the sticking of molecules at the liquid interface.

II. WETTED-WHEEL STUDIES OF F ATOM REACTIVE SCATTERING FROM LIQUID SQUALANE

As a first example, we discuss high-resolution IR laser studies of F atom scattering from squalane, which forms rovibrationally excited HF(ν ,J) via the highly exothermic ($\Delta H \approx -38$ kcal/mol) H atom abstraction reaction at the liquid hydrocarbon interface (Figure 1). ^{2,22} The fluorine beam is based on

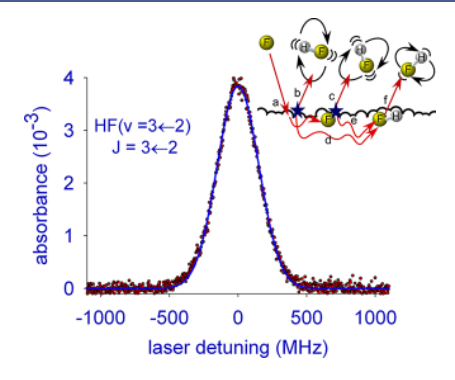


Figure 1. Sample data for F atom reactive scattering from a liquid squalane surface, probed by direct absorption on the HF(ν = 3 \leftarrow 2) R(2) fundamental ($\Delta\nu$ = +1) transition with a high-resolution tunable color-center laser. Note that the lower state contains 25 kcal/mol vibrational energy and is far out of equilibrium with the 300 K surface. Adapted with permission from refs 2 and 22. Copyright 2006 and 2008 American Institute of Physics.

a "mini-slit" source (0.3 cm \times 0.03 cm), whose orifice is pulsed to 800 V during a 2 ms gas pulse of 5% F₂/rare-gas mixture, with the discharge dissociating \sim 25% of the fluorine molecules into F atoms. The experiment is carried out in an \sim 125 L diffusion-pumped vacuum chamber at base pressures of 10^{-6} Torr (Figure 2), in excess of the \sim 10⁻⁷ Torr vapor pressure of liquid squalane. Peak gas (F, F₂, rare gas) densities at the liquid surface are <1.5 \times 10¹³/cm³, translating into mean free paths 2

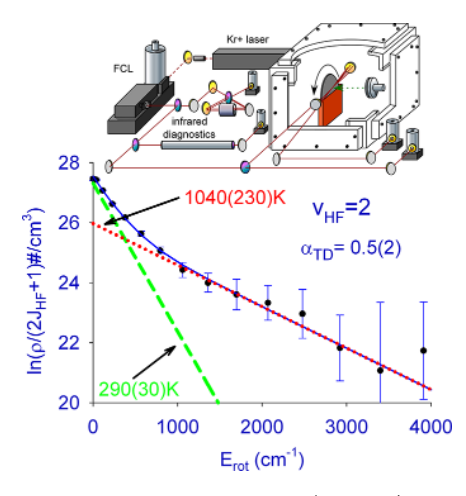


Figure 2. Boltzmann plot of the $HF(\nu=2,J)$ quantum-state populations as a function of rotational energy. Note the clear kink in the curve near 350 cm⁻¹, which corresponds to a crossing between room temperature (290 K) and rotationally hyperthermal (1040 K) distributions, attributed to "microscopic branching" between trapping—desorption (TD) and impulsive reactive scattering (IS) channels. Top panel displays a schematic of the experimental rotating-wheel apparatus. Adapted with permission from refs 2 and 22. Copyright 2006 and 2008 American Institute of Physics.

orders of magnitude greater than the ~ 1 cm distances between liquid and the infrared laser probe axis. HF(ν ,J) product molecules recoiling from the gas—liquid interface are detected on the $\Delta \nu = +1$ fundamental via direct infrared absorption spectroscopy, using a high-resolution color-center laser ($\Delta \nu \approx 3$ MHz), multipassed 16 times above the liquid in a Herriot cell. Absorption sensitivities down to the 10^8 HF/quantum state level are limited primarily by quantum shot noise on the photon arrival times. Such high sensitivities are obtained by differential detection on matched InSb detectors and active servo-loop stabilization of the laser amplitude.

The time-dependent HF absorption (or stimulated emission) signals are captured by a transient digitizer in a 200 μ s window centered on the F atom pulse. The laser frequency is incremented between gas pulses, yielding highresolution Doppler absorption profiles out of a lower $HF(\nu,J)$ quantum-state, with calibration of the frequency scan calibration by recording laser transmission through a Fabry-Perot etalon. To establish an intensity reference, the HF(ν = $3 \leftarrow 2$; $J = 3 \leftarrow 2$) transition is recorded multiple times daily, with measurements on the full $HF(\nu,J)$ manifold normalized for fluctuations in the F atom source. Signal-to-noise ratio on nascent Doppler profiles is >20:1, with an integrated S/N > 200 (see Figure 1). At Doppler-limited resolution ($\Delta \nu_{\mathrm{Doppler}}$ (300 MHz) $\gg \Delta \nu_{\rm laser}$ (3 MHz)), each HF rovibrational transition appears as an isolated line, with peak quantum-state densities of $\sim 10^{10}$ HF/cm³. The HF($\nu = 3 \leftarrow 2$, $J = 3 \leftarrow 2$) translational Doppler profiles are well fit by a broadened Gaussian line shape, characteristic of superthermal recoil velocity distributions parallel to the laser probe axis and consistent with Doppler line shapes hotter than the liquid surface $(T_{\text{trans}} > T_{\text{S}})$. The data yield integrated absorption intensities for each spectral line, with the observed spectra fit by nonlinear least-squares analysis to obtain absolute HF(v,J)state-resolved column densities.

Sample rotational populations for the HF(ν = 2, J) manifold are displayed in Figure 2, which exhibits a pronounced "kink"

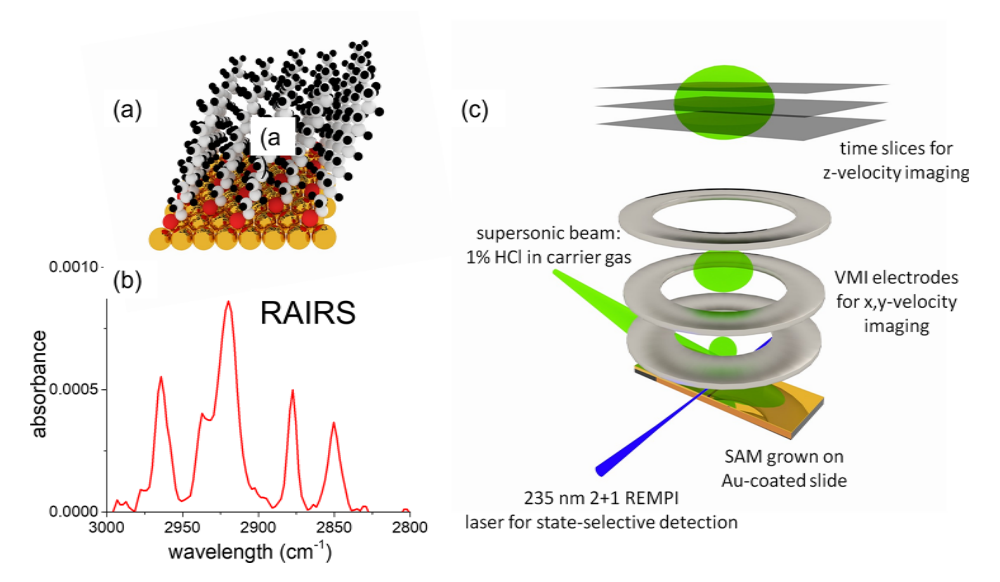


Figure 3. Schematic diagram for quantum-state-resolved scattering of HCl from (a) dodecane self-assembled monolayers (SAMs) on a gold surface, (b) with surface characterized by reflection—absorption infrared spectroscopy (RAIRS), and (c) detected via photoionization and 3D velocity map imaging. Adapted with permission from ref 1. Copyright 2016 American Chemical Society.

near $E_{\rm rot} \approx 350~{\rm cm}^{-1}$. Such deviations from a linear Boltzmann plot are highly reminiscent of "dual-temperature" J-progressions noted for many closed-shell (CO₂, OCS, DCl) molecular projectiles inelastically scattered from liquids in other studies. Similar behavior has been often seen in translational TOF mass spectroscopy studies and attributed to "microscopic branching" between trapping-desorption (TD) and impulsive scattering (IS) channels, where the former reflects complete loss of collisional memory and thermal equilibration to T_S , while the latter contains all information on non-equilibrium energy transfer dynamics. We tentatively associate (but confirm below) these hot and cold rotational HF(v,J) channels as quantum-state-resolved evidence for a similar "microscopic branching" of products arising from strongly exothermic chemical reaction at the gas—liquid interface.

We quantify the reactively formed HF rotational populations by a two-temperature Boltzmann least-squares fit:

$$\rho_{\nu}(J) = A_{\rm TD} \exp(-E_{\rm rot}(J)/kT_{\rm TD}) + A_{\rm IS} \exp(-E_{\rm rot}(J)/kT_{\rm IS})$$

$$\tag{1}$$

where $\rho_{\nu}(J)$ is the column integrated density of HF(ν ,J), $E_{\text{rot}}(J)$ is the rotational energy, k is the Boltzmann constant, and $T_{\rm TD}/$ $T_{\rm IS}$ and $A_{\rm TD}/A_{\rm IS}$ represent the temperatures and amplitudes of the TD and IS distributions, with additive contributions from cooler (TD) and hotter (IS) Boltzmann temperature components well represented by dashed and dotted lines, respectively. Note in particular that the lower temperature component (290(30) K) is in good agreement with roomtemperature (300 K) squalane and indeed consistent with a fractional portion of the HF product recoiling from the surface via a fully rotationally thermally accommodated TD channel. In the context of this simple two-temperature model, such agreement provides the first quantum-state-resolved support for microscopic branching between trapping-desorption (TD) and impulsive scattering (IS) pathways, even for highly exothermic reactive events at the gas-liquid interface.

It is worth noting that the existence of a room-temperature TD component for rotation does *not* imply thermal accommodation with respect to HF vibration; indeed, Figure

2 represents data from rotational populations in the vibrationally excited HF(v = 2) manifold, i.e., ≈ 25 kcal/mol above the ground state energy and obviously highly nonthermal. This model therefore also establishes clear limits on time scales for such chemically reactive trapping-desorption dynamics, specifically that the recoil be sufficiently slow for partial rotational equilibration with the liquid surface but not yet long enough for vibrational accommodation. (We of course cannot yet specify precisely what "sufficiently slow" and "long enough" mean, but gas phase rotational and vibrational collisional relaxation numbers of 10 and 10000 would imply a 10 ps to 10 ns window.) More quantitatively, the branching ratio between TD and IS events can be calculated by summing over their respective contributions in eq 1, yielding an accommodation coefficient $\alpha = 0.5(2)$ for the HF($\nu = 2$) manifold. Thus, only 50% of the HF($\nu = 2$) product desorbs after rotationally equilibrating with the liquid interface, implying $au_{
m desorb} pprox au_{
m rot ext{-}relax}$ $\ll au_{
m vib-relax}$ and consistent with the wealth of data indicating much shorter time scales for rotationally vs vibrationally inelastic scattering in the gas phase.³⁸ However, this is only one of many quantum-state-resolved reaction systems possible to investigate with laser methods at the gas-liquid surface, insights from which should eventually provide us with a much more complete dynamical story. The key result worth stressing is that exothermic reactive scattering at the gas-liquid interface can result in highly nonequilibrium distributions of internal (vibrational/rotational) and translational states, despite the enormous vibrational state densities of the liquid in nanometer-scale proximity with the recoiling molecular projectile.

III. STATE-RESOLVED SCATTERING FROM SELF-ASSEMBLED MONOLAYER (SAM) LIQUID MIMETICS

One powerful alternative to wetted-wheel methods involves preparation of "liquid-like" surfaces chemically attached to a substrate, specifically self-assembled monolayers (SAMs) of organic thiols (R–SH) bound to a Au surface by covalent Au—S linkages (Figure 3a). We have performed preliminary

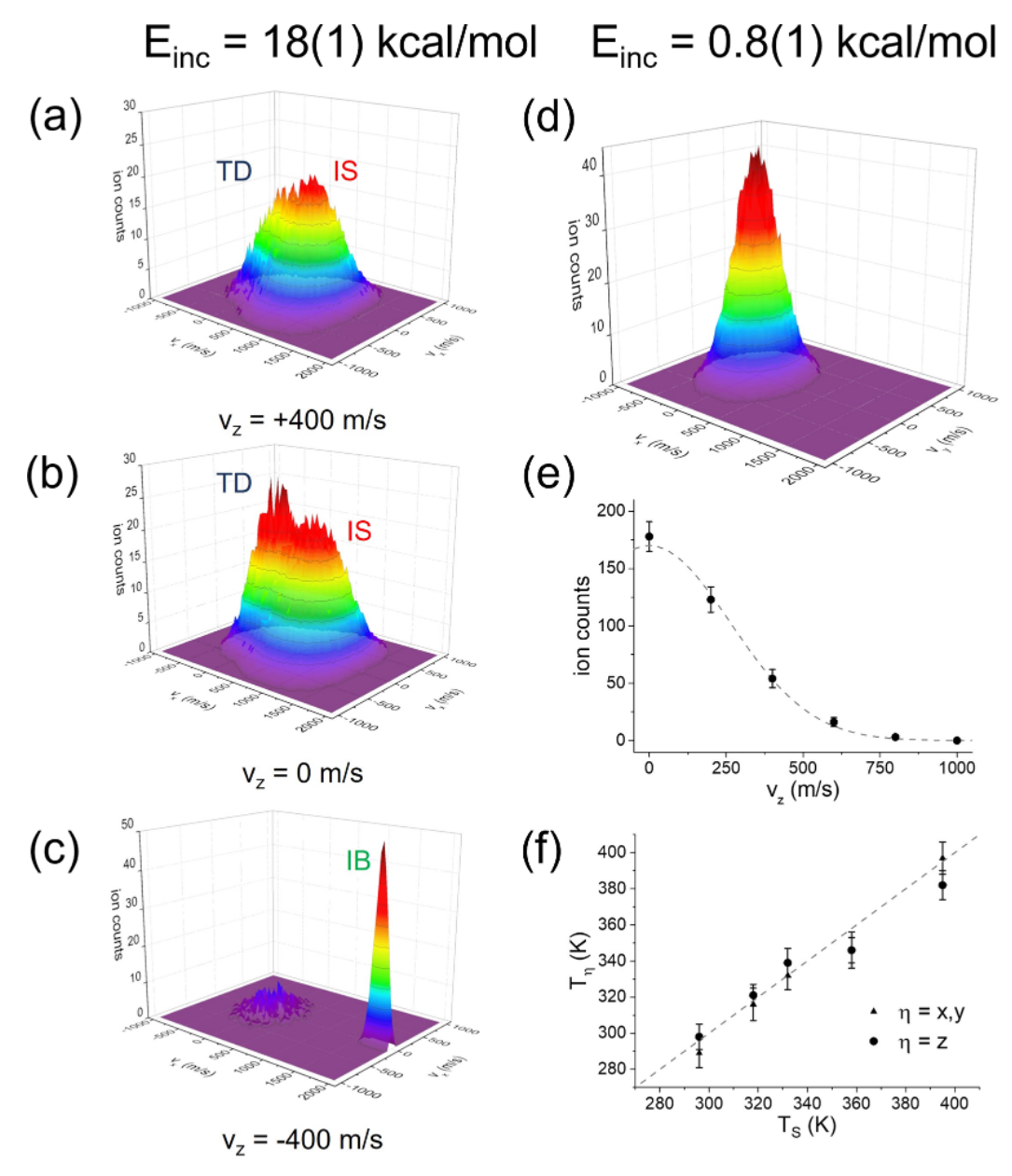


Figure 4. Sample 2D VMI data for hyperthermal HCl scattering ($E_{\rm inc}$ = 18(1) kcal/mol) from dodecane SAMs revealing both TD (axisymmetric) and IS (forward scattered) contributions. The left panels capture three different slices from (a) $v_z \approx 400$ m/s and (b) $v_z \approx 0$ m/s and (c) with the supersonic beam cleanly separated by negative $v_z \approx -400$ m/s incident component. The right panels reflect low-energy HCl scattering ($E_{\rm inc}$ = 0.8(1) kcal/mol) and reveal (d) pure TD scattering with (e, f) translational (x, y, z) temperatures in excellent agreement with T_S . Adapted with permission from ref 1. Copyright 2016 American Chemical Society.

quantum-state-resolved scattering of thermal and hyperthermal HCl projectiles from such self-assembled monolayers, comprised of dodecane (C_{12}) aliphatic chains and made from standard synthetic methods. ^{39,40} Well-formed SAMs with reproducible local structure in each aliphatic chain can be distinguished by four reflection/absorption IR (RAIRS) peaks corresponding to methyl and methylene CH stretching vibrations (see Figure 3b). After such RAIRS characterization, these SAM samples are placed in a vacuum chamber maintained at 5 \times 10 $^{-9}$ Torr by one 1250 L/s and two 250 L/s turbo pumps, with a cartridge heater to warm the sample between 294 K and 450 K. Repeated RAIRS measurements indicate that such C_{12} SAMs can withstand heating to 450 K under vacuum for up to 3 days without deterioration.

The SAM surfaces are probed by grazing-angle (75°) inelastic HCl scattering with quantum-state- and velocity-resolved detection (Figure 3c). Specifically, 1% mixtures of HCl seeded in buffer gas diluent are released through a $100~\mu m$ pinhole orifice pulsed valve 41 (200 μs duration, 10 Hz repetition rate) and pass through a 2 mm skimmer 80 mm downstream to produce a narrow spread ($v/\Delta v=10$) of transverse velocities (<3%) at the gas–SAM interface, with >90% of the incident beam HCl molecules cooled into J=0 rotational state. The HCl(v=0, J>0) molecules resulting from rotationally inelastic scattering at the gas–SAM interface are then ionized via 2+1 REMPI^{42,43} with 235 nm light from the frequency-tripled output of a Nd:YAG-pumped pulsed dye laser, achieving state-selective ionization of HCl(v=0, J=0–

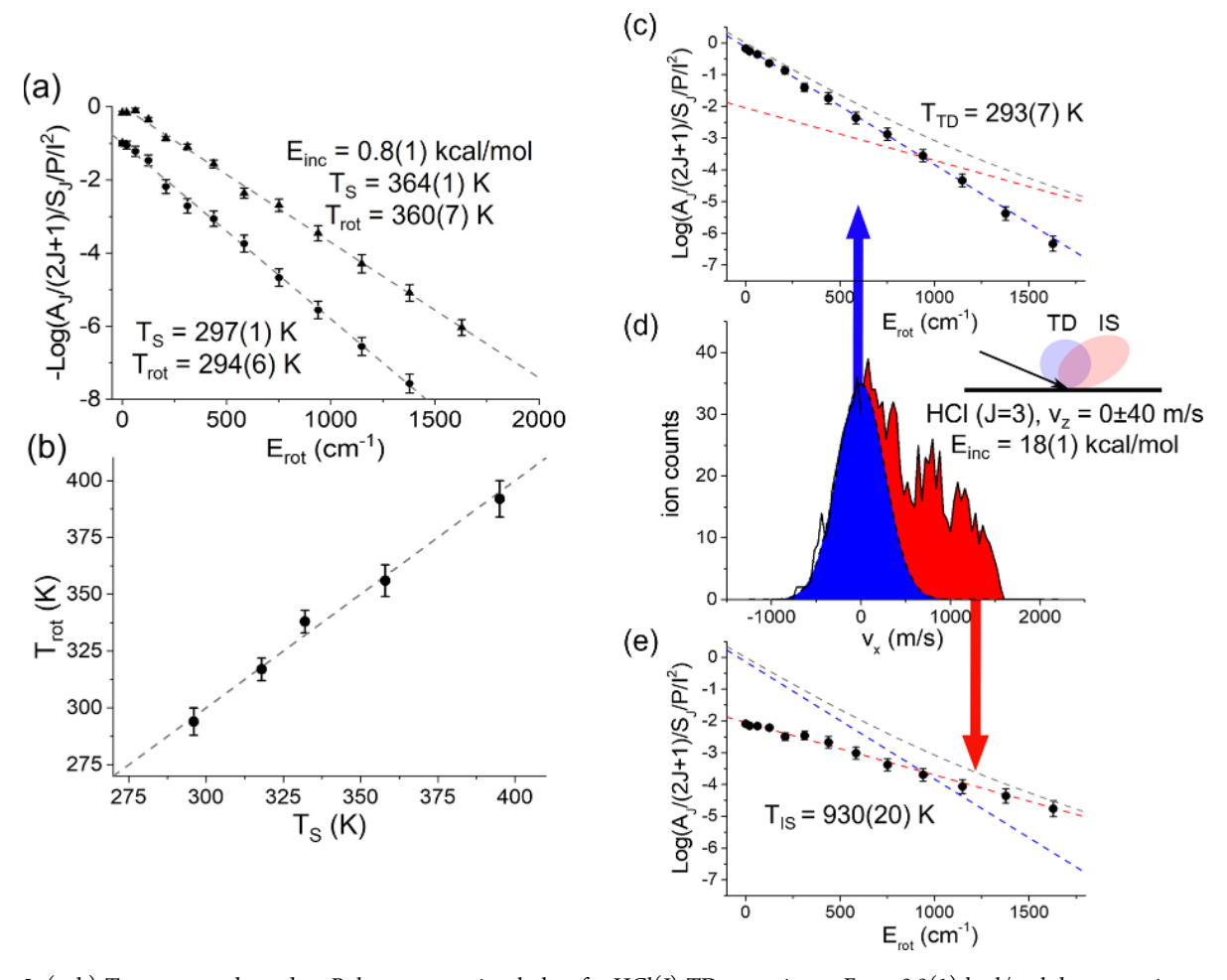


Figure 5. (a, b) Temperature-dependent Boltzmann rotational plots for HCl(J) TD scattering at $E_{\rm inc}=0.8(1)$ kcal/mol demonstrating complete thermal equilibration between $T_{\rm rot}$ and $T_{\rm S}$. (c, e) For hyperthermal scattering ($E_{\rm inc}=18(1)$ kcal/mol), J-dependent fluxes are extracted from symmetrized VMI fits (d) to the back half-plane ($\nu_x<0$) distribution (blue), with IS fluxes (red) obtained by subtraction. Note that VMI analysis allows novel extraction of J-state TD/IS fluxes *irrespective of rotational distributions* and thereby providing completely independent support for a dual-temperature kinetic model. Adapted with permission from ref 1. Copyright 2016 American Chemical Society.

14) molecules with a well specified final J. As depicted in Figure 3c, the ionization occurs along the central stack of a velocity map imaging system, 30,44-46 with the gold substrate acting as a repeller electrode. The stack extracts ions from the ionization region through a 50 cm vertical flight tube onto a 2D position-sensitive (v_x, v_y) microchannel plate (MCP) detector, where the amplified electron pulse strikes a phosphor screen imaged by a CCD camera, with arrival time determining the ion v_z component. So Voltage across the MCP is gated between 1300 V (\approx 0 gain) and 1700 V (\approx 10⁷ gain) for a tunable "DC-slice" of the ion cloud arrival times. The VMI (ν_{xy} v_{ν} , v_{z}) is calibrated by imaging residual HCl molecules equilibrated to the chamber walls, with thermal fits permitting the velocity origin and v_x , v_y scale factor on the MCP to be accurately determined. These calibration measurements are repeated multiple times per day to monitor/correct for any minor drift in the origin or scaling of the velocity map images.^{29,30}

The ability to resolve the velocity component along the surface normal allows systematic elimination of ion signals arising from the incident beam. The value of such temporal separation is specifically illustrated in Figure 4, where the strong incident beam signal (Figure 4c) appears in only a single velocity slice ($v_z \approx -400 \text{ m/s}$), while the scattered ions

(Figures 4a,b) form broader 2D structures spanning multiple slices ($v_z \ge 0$). These 3D velocity-space images also nicely geometrically differentiate between TD and IS scattering channels. Specifically, as the TD contributions have lost all memory of the incident collision with the SAM surface, the corresponding signals are centered around $v_x = v_y = 0$, whereas the IS channel is strongly forward peaked in the incident beam direction ($v_x \gg 0$). Similarly, the TD signals peak at small $v_z \approx 0$, whereas the IS scattered molecules preferentially recoil with larger $v_z > 0$. This ability to achieve separation of incident beam (IB) and scattered signals (TD, IS) is crucial and permits quantitative normalization of any differential changes in state-resolved scattered fluxes.

We first consider the 3D angular/flux distributions of scattered HCl doped into a slow Ar supersonic beam, for which the incident HCl molecules are expected to be TD dominated and equilibrate to $T_{\rm S}$ with 100% efficiency. Specifically, provided that the probability (α) of a molecule trapping long enough to lose memory is independent of incident energy, angle, or internal quantum-state, then detailed balance considerations demand the desorbing molecules to emerge in a Maxwell–Boltzmann distribution at $T_{\rm S}$, with velocity space densities described by a 1D Gaussian restricted to the upper half-plane ($\nu_z > 0$). Figure 4 (right panel) presents

a summary of desorbing velocity distributions for incident HCl seeded in argon ($E_{\rm inc}=0.8(1)$ kcal/mol) and colliding with C_{12} -SAM at room temperature. The distributions are analyzed with 1D ($\nu_z>0$, Figure 4e) and 2D Gaussian (ν_x,ν_y) fits, which yield full width at half-maximum (fwhm) values each in excellent agreement with $T_{\rm S}$. By way of additional confirmation, these measurements have been replicated as a function of $T_{\rm S}$, with results (Figure 4f) in quantitative agreement over $T_{\rm S}=294-400$ K. Such agreement between $T_{x,y}$, T_{z} , and $T_{\rm S}$ values strongly supports our basic model that scattering at low incident energies is dominated by trapping—desorption (TD) and complete thermal equilibration. By detailed balance considerations, this implies near-unity trapping probabilities with respect to the incoming HCl for all speeds sampled typically at $T_{\rm S}$.

However, state-selective REMPI/DC-slice VMI capabilities allow us to take this analysis much further, as we know and can therefore integrate over the full 3D velocity distributions. Specifically, in addition to detailed vector information on 3D translational degrees of freedom, the scattered HCl can also be characterized by scalar rotational distributions. 30,42,43 Figure 5a displays sample Boltzmann plots of recoiling rotational distributions integrated over all 3D velocities and for low (291(1) K) and high (364(1) K) liquid temperatures, which are well fit to a single Boltzmann temperature (T_{rot}) in excellent agreement with T_S . By way of confirmation, this procedure is again repeated over a series of temperatures (Figure 5b), with results consistent with $T_{\rm rot} \approx T_{\rm S}$ over the full range of temperatures explored. The panels in Figures 4 and 5 represent compelling evidence that low energy HCl colliding with SAMs (i) stick with unit probability independent of rotational quantum-state and (ii) desorb with both rotational and translational degrees of freedom in equilibrium with the surface temperature.

With both the translational/rotational populations well characterized for pure TD scattering conditions, we can now consider nonequilibrium impulsive scattering (IS) events at higher $E_{inc.}$ The cleanest operational definition of the IS channel is that it comprises all deviations from pure TD behavior. Particularly for grazing 75° incidence, IS contamination in the back scattered half-plane should be negligible; thus one should be able to isolate the pure TD channel (blue) by performing half Gaussian fits exclusively to $v_x < 0$ scattering events. As shown in Figure 5d, pure IS velocity distributions (red) can then be obtained by difference between total VMI signals and these TD fits symmetrically extended into $v_x > 0$. Simply summarized, 2π -steradian VMI methods offer a novel capability for independent separation of 3D scattering flux contributions into TD and IS channels as a function of internal rovibrational quantum-state.

As a powerful corollary, we can therefore also integrate these TD and IS channels over all final 3D velocities to obtain scalar rotational populations of the scattered HCl molecules. It is worth stressing that analysis of rotational populations arising from combined TD and IS scattering channels frequently invoke a dual-temperature rotational distribution, with one temperature fixed at $T_{\rm TD} \approx T_{\rm S}$ and $T_{\rm IS}$ allowed to float, assuming a hotter, albeit Boltzmann-esque IS rotational distribution. The considerable advantage of 3D velocity map imaging is that it allows deconstruction of each J-state-resolved image into TD and IS components, without any assumptions on the rotational distributions, and in this way permits independent validation of such a dual-temperature

analysis. For example, Figure 5c,e display sample Boltzmann plots for J populations extracted separately from integrated TD and IS velocity distributions. Least-squares fits to the isolated TD populations return a temperature ($T_{\rm TD} \approx 293(7)$ K) in excellent agreement with the measured SAM surface and indeed as expected for fully thermally equilibrated interactions. Most remarkably, the IS rotational populations also exhibit linear Boltzmann plots, with a hyperthermal temperature-like distribution quantitatively consistent with "dual-temperature" analysis of the total quantum-state populations. Finally, it is worth stressing that this unexpected simplicity in the IS rotational distributions does not require any simplifying assumptions in the corresponding velocity distributions, which from Figure 4a,b are in fact highly anisotropic and strongly forward-scattered in the near-specular direction. Hence, the agreement between $T_{\rm TD}$ and $T_{\rm S}$ temperatures (in both rotation and translation) is profoundly surprising and suggests the presence of additional constraints in inelastic scattering dynamics at the gas-liquid interface. Though these studies are preliminary, they do indicate the remarkable versatility of REMPI/VMI scalar and vector scattering from "chemically tunable" SAM surfaces as a powerful tool for quantum-state-resolved energy-transfer/reaction kinetics at liquid-like interfaces.

IV. EVAPORATION DYNAMICS AT THE GAS-LIQUID WATER MICROJET INTERFACE

As a final topic, we turn to the use of microjets for gas-liquid interfacial studies. Microjets of pure water and moderately viscous hydrocarbons⁴⁹ have been successfully used in studies where high-vacuum conditions are required, including X-ray⁵⁰ and photoelectron⁵¹ spectroscopy of the solutes and liquids themselves, as well as time-of-flight (TOF) studies of molecular solutes as large as acetic acid dimer (CH₃COOH)₂. ⁵² Of particular relevance to the present work are the TOF studies by Nathanson and co-workers on nonequilibrium "expulsion" dynamics of noble-gas atoms and small molecules. ^{49,53} Interestingly, surprisingly little attention has been devoted to the internal-quantum-state distributions of molecular evaporants. Studies by Weber of low vapor pressure liquid metals, such as Na_2 evaporating from molten sodium, have been performed. There have been studies by Buntine and co-workers using resonance-enhanced multiphoton ionization (REMPI) for detection of benzene evaporating from water-ethanol mixtures,55 as well as Barinkova using laser-induced fluorescence (LIF) for detection of aromatic compounds laser-ablated from a microjet.⁵⁶ However, due to dense rotational structure of these large organic molecules, only rotational envelopes of partially overlapping vibrational bands could be observed.

To address more detailed dynamical questions, we have recently developed methods for quantum-state-resolved studies of NO expulsion from liquid water microjets, exploiting LIF detection for high-sensitivity characterization of nascently evaporated spin—orbit, rotational, and Λ -doublet states. This work builds naturally on previous studies in our laboratory for quantum-state distributions of NO scattering from low-vapor-pressure liquids ^{48,57–61} but now extended to a much higher vapor pressure "solvent" (H₂O) of crucial importance. Specifically, these studies are performed in a vacuum chamber pumped with a 1200 L/s turbomolecular pump through a liquid-nitrogen cryogenic baffle (see Figure 6). With the microjet in operation, the working pressure in the chamber is

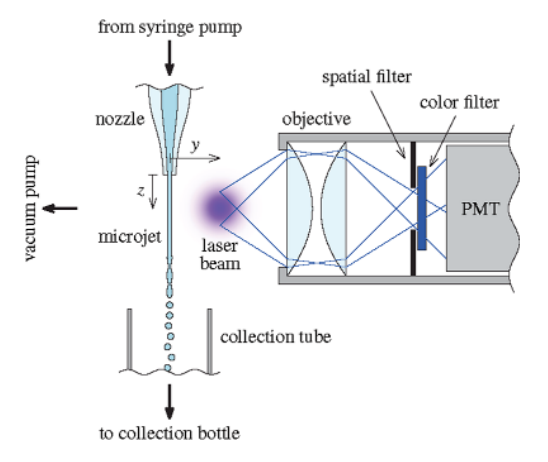


Figure 6. Schematic drawing of the experimental microjet apparatus, based on laser-induced fluorescence (LIF) to probe quantum-state-resolved NO evaporating from a liquid-water surface. The down-stream distance z is measured vertically from the nozzle exit, with the radial distance y measured horizontally from the jet axis toward the LIF detection region. Adapted with permission from ref 3. Copyright 2019 American Institute of Physics.

 $\leq 10^{-5}$ mbar, resulting in mean free paths many times larger than the chamber dimensions. Solutions are prepared by dissolving NO into H₂O at 2.7 bar (2000 Torr) in a stainlesssteel mixing cylinder, resulting in an ~5 mM solution, and transferred to a syringe pump. The (vertical) liquid microjet is generated by pumping the solution at high pressure through a quartz nozzle drawn from capillary tubing and mounted in an HPLC filter with 0.5 μ m pore size. The filter itself is mounted to an XYZ translational stage such that the nozzle orifice can be precisely positioned with respect to the probe laser (Figure 6). Besides protecting the nozzle from clogging due to trace particulates, the filter also controls the microjet temperature, achieved by pumping coolant through a metal coil soldered to the filter and monitoring the body temperature (T_f) with ± 0.5 $^{\circ}$ C accuracy. For an \sim 4 μ m nozzle exit diameter, the flow rate at pressures ≥100 bar is ~0.1 mL/min, resulting in typical jet speeds of ~ 100 m/s. Under these conditions, the laminar flow length is ≥1 mm, after which the jet breaks into a stream of droplets due to Plateau-Rayleigh instability. 62 The droplets are then collected and frozen at the bottom of the vacuum chamber in a glass bottle submerged in liquid nitrogen.

NO molecules evaporating from the liquid microjet are excited on the $A^2\Sigma(\nu'=0,J',\varepsilon')\leftarrow X^2\Pi_{1/2,3/2}(\nu''=0,J'',\varepsilon'')$ band by a pulsed tunable UV output of a frequency-tripled dye laser operating with a 10 Hz repetition rate. The resulting $A^2\Sigma(\nu'=0)\to X^2\Pi(\nu'')$ fluorescence is monitored by a photomultiplier tube (PMT) perpendicular to both microjet and laser-beam axes at the center of the chamber. The PMT signals are integrated over a 500 ns window and normalized to pulse energy on a shot-to-shot basis. All LIF spectra are taken with pulse energies $\lesssim\!\!0.5~\mu\mathrm{J}$ to ensure excitation in a linear regime.

Figure 7 (lower panel) displays a typical LIF spectral region for NO evaporating from a Ø4.4 µm liquid microjet, with quantum-state populations extracted by a weighted least-squares fitting based on line positions and absorption coefficients from the LIFBASE model. Sample Boltzmann plots obtained from these populations are displayed in Figure 7 (upper panel), for which the rotational levels within each spin—orbit manifold are described remarkably well by a single

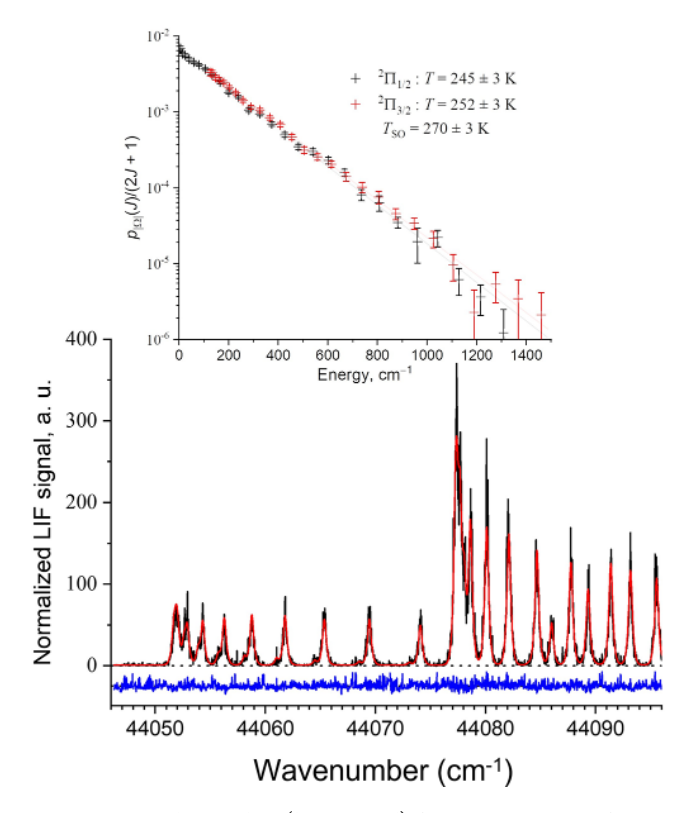


Figure 7. Sample LIF data (lower panel) for NO evaporating from a $\emptyset 4.4~\mu m$ water microjet (probe at z=1~mm,y=2~mm): experimental fluorescence data (black) normalized to laser pulse energy, least-squares fit (red), and normalized residuals (blue). Rotational populations (upper panel) for each spin—orbit manifold reveal excellent linear Boltzmann plot behavior, but at temperatures notably ($\Delta T \approx 20{-}30~K$) lower than the microjet surface (272(4) K). Adapted with permission from ref 3. Copyright 2019 American Institute of Physics.

temperature, $T_{\rm rot}$. Of particular dynamical interest, the NO rotational temperatures (Figure 7) are significantly *cooler* (\sim 50 K at $T_{\rm jet}=285$ K) than the corresponding microjet temperatures and even exhibit trends in qualitative opposition (see Figure 8). The central issue is whether such data necessarily reflect *nonequilibrium evaporation dynamics* of NO from the water microjet. This proves to be a hard issue to address, with our best answer described below!

The microjet literature has tended to follow the tradition of estimating collisional impact from the "number of collisions" (N_0) along a straight line from the jet to the detection region. This number can be estimated as $N_0 \sim n_0 \sigma r_0$, where n_0 is the surface vapor density, r_0 the microjet radius, and σ an effective cross-section for collisions between NO and co-evaporating H_2O , the argument being that if $N_0 < 1$, the effect of collisions can be neglected. This approach, however, does not take into account simultaneous evaporation of the water microjet, which has two effects. The first is that evaporation cools the microjet, an effect which can be readily calculated and incorporated into measurement with our measurement of the bulk microjet temperature. A second and more important effect is that the vapor pressure for water is quite high (multiple Torr), with mean free path lengths at the microjet surface short enough to induce additional cooling by an adiabatic expansion(i.e., supersonic) expansion.⁶⁴ Simply stated, the water vapor cools like a gas expanding through a 1D "slit" orifice due to the 1/r

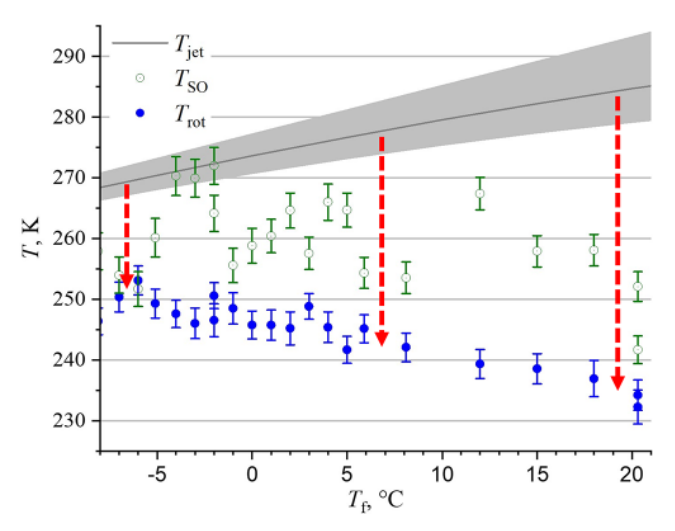


Figure 8. NO Boltzmann parameters for a Ø4.4 μ m microjet (z=1 mm, y=2 mm) as a function of filter temperature $T_{\rm f}$. Rotational ($T_{\rm rot}$) and spin—orbit ($T_{\rm SO}$) temperatures in blue and green, respectively. Most notably, the observed rotational and spin—orbit temperatures are strongly out of equilibrium from the water microjet temperatures (gray) predicted from evaporative cooling in the $0 \le z \le 2$ mm range. Adapted with permission from ref 3. Copyright 2019 American Institute of Physics.

dropoff in density away from the microjet, which can collisionally transfer and/or remove energy from the coexpanding NO. In order to more reliably interpret the apparent nonequilibrium differences between NO evaporant and microjet temperatures, we have developed a simple analytic model for collisional equilibration of the nascent NO with the much denser adiabatically cooled stream of co-evaporating H_2O molecules. The details of this analytic treatment are mathematically intriguing and described in detail elsewhere but are not particularly relevant to the theme of this Account; thus we leave the derivation to the interested reader and simply quote the simple analytical expression for the final average NO temperature:

$$\langle T_{\text{NO}} \rangle = T_0 \left\{ R^{n_0 \sigma r_0} + \frac{n_0 \sigma (r_d R^{\gamma} - r_0 R^{n_0 \sigma r_0})}{n_0 \sigma r_0 - \gamma + 1} \right\}$$
(2)

where $R \equiv r_0/r_{\rm d}$ is the ratio of the microjet radius to the radius $r_{\rm d}$ at which NO is detected and $\gamma = C_{\rm P}/C_{\rm V}$ is the heat capacity ratio. It should be noted that σ in eq 2 reflects an *effective* cross-section for rotationally equilibrating NO with the coexpanding H_2O .

 $\langle T_{\rm NO} \rangle$ values calculated from eq 2 are plotted in Figure 9 as a function of $T_{\rm jet}$ for a range of σ values and parameters $r_0 \approx 2.2~\mu$ m, $r_{\rm d} \approx 2$ mm appropriate to the present experimental conditions. Interestingly, the observed deviation of $\langle T_{\rm NO} \rangle$ from $T_{\rm jet}$ is correctly predicted to be larger for a warmer $T_{\rm jet}$ due primarily to the strong temperature dependence of the initial water-vapor density $n_0(T_{\rm jet})$. However, by far the most striking observation in Figure 9 is that both experimental results and curvature for the $\langle T_{\rm NO} \rangle$ dependence on $T_{\rm jet}$ can be well reproduced with an effective collision cross-section of only σ = 13 Ų, i.e., more than an order of magnitude smaller than estimates based on total N_2 – H_2 O and H_2 O– H_2 O collision cross-sections. Such differences probably reflect that it requires multiple collisions to fully equilibrate NO to the H_2 O gas temperature. Nevertheless, the model predicts that even

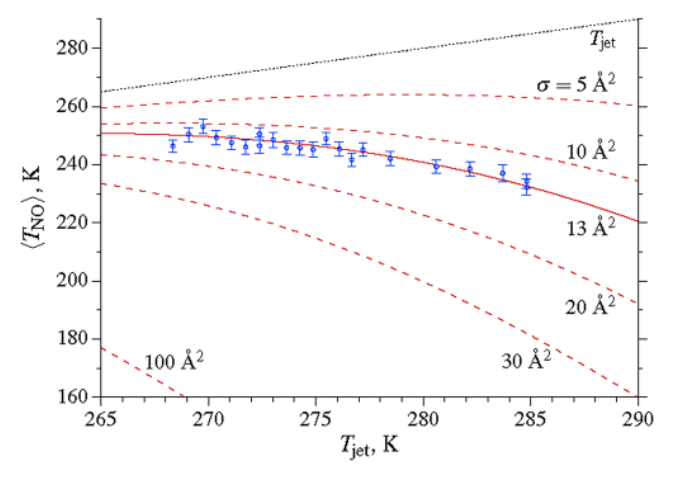


Figure 9. A more sophisticated cooling model for NO due to postevaporative collisions in an adiabatically expanding/cooling water vapor, calculated for a range of effective cross-sections. The blue points with error bars represent the experimental $T_{\rm rot}$ values from **Figure 8.** Note the remarkable agreement in both experimental magnitudes and $T_{\rm jet}$ dependence trends based on a modest energy-transfer cross-section ($\sigma=13$ Ų) for collisional equilibration. Adapted with permission from ref 3. Copyright 2019 American Institute of Physics.

rather modest collisional cross-sections can lead to appreciable cooling effects, even for $N_0 \sim n_0 \sigma r_0 \lesssim 1$.

We have demonstrated first fully quantum-state-resolved measurements for internal-state distributions of molecules evaporating from a liquid microjet, specifically, NO dissolved in water. As the key observation, the NO state distributions are found to be well described by rotational and spin-orbit temperatures significantly lower (by as much as 50 K) than the liquid surface for the range of temperatures studied (267-285 K). However, a deeper analysis reveals that these observations could also be consistent with NO evaporating in thermal equilibrium with the microjet surface but impacted by cooling due to collisions with adiabatically co-expanding water vapor prior to detection. Our results indicate that a further order-ofmagnitude reduction in collision probability will be required to unambiguously confirm nonequilibrium solute-gas expulsion dynamics at the gas-liquid interface. Nevertheless, these considerations already lead us to conclude that even relatively small collision probabilities exert significant effects on the observed internal-state distributions and that results of previous experiments where collisional effects have been ignored based on an estimate of $N_0 \lesssim 1$ may require a more careful reinterpretation.

AUTHOR INFORMATION

Corresponding Author

David J. Nesbitt — JILA, National Institute of Standards and Technology and University of Colorado, Boulder, Colorado 80309, United States; Department of Physics and Department of Chemistry, University of Colorado, Boulder, Colorado 80309, United States; orcid.org/0000-0001-5365-1120; Email: David.Nesbitt@colorado.edu

Authors

ı

Alex M. Zolot – Quantinuum, Broomfield, Colorado 80021, United States Joseph R. Roscioli – Aerodyne Research, Inc., Billerica, Massachusetts 01821, United States

Mikhail Ryazanov – JILA, National Institute of Standards and Technology and University of Colorado, Boulder, Colorado 80309, United States; orcid.org/0000-0002-7269-6436

Complete contact information is available at: https://pubs.acs.org/10.1021/acs.accounts.2c00823

Author Contributions

CRediT: David J. Nesbitt conceptualization (lead), data curation (equal), formal analysis (equal), funding acquisition (lead), methodology (lead), validation (equal), visualization (equal), writing original draft (lead), writing-review & editing (lead); Alexander M. Zolot conceptualization (supporting), data curation (supporting), writing, review & editing (supporting); Joseph Robert Roscioli data curation (supporting), investigation (supporting), writing-review & editing (supporting); Mikhail Ryazanov conceptualization (supporting), data curation (lead), formal analysis (lead), investigation (lead), writing original draft (supporting), writing, review & editing (supporting).

Notes

The authors declare no competing financial interest.

Biographies

David J. Nesbitt is a faculty member at the University of Colorado, Departments of Chemistry and Physics, JILA, and the National Institute of Standards and Technology (NIST).

Alex M. Zolot is Lead System Engineer, Technology Development Division at Quantinuum, LLC.

Joseph R. Roscioli is Principal Scientist at Aerodyne Inc. using highresolution IR spectroscopy to explore greenhouse gas isotopes in soil gases.

Mikhail Ryazanov has a Ph.D. from the University of Southern California with Hanna Reisler. His research in Boulder has focused on developing novel methods for quantum-state-resolved evaporation studies in liquid microjets.

ACKNOWLEDGMENTS

Funding for this work has been provided by the National Science Foundation under grant CHE-1665271/2053117 from the Chemical, Structure, Dynamics and Mechanisms-A Program (CSDM-A), with additional support for apparatus construction from PHY-1734006 (Physics Frontier Center Program) and Air Force Office of Scientific Research (FA9550-15-1-0090). Many hard working graduate students, postdocs, and visiting professors over the past 15+ years have contributed to the work herein, including Bradford Perkins (who was there at the very beginning and stimulated the whole Nesbitt group fascination with quantum-state gas-liquid dynamics), Warren Harper and Paul Dagdigian (who participated crucially in the reactive F + squalane studies), Carl Hoffman and Brian Riggs (for their diligent efforts in developing/improving the HCl/SAMs scattering studies with REMPI and VMI techniques), Andy Gisler and Timothy Livingston Large (who extended the IR detected scattering studies to more complex liquids and/or polyatomic projectiles), and finally Amelia (Mia) Zutz and Mike Ziemkiewicz (who developed LIF detection methods for scattering open

shell NO molecules from RTILs and hot molten metals). The authors are profoundly grateful to each of these group colleagues for their manifold efforts, without which this Account would simply not be possible to write.

REFERENCES

- (1) Hoffman, C. H.; Nesbitt, D. J. Quantum state resolved 3D velocity map imaging of surface-scattered molecules: Incident energy effects in HCl + self-assembled monolayer collisions. *J. Phys. Chem. C* **2016**, *120*, 16687–16698.
- (2) Zolot, A. M.; Harper, W. W.; Perkins, B. G.; Dagdigian, P. J.; Nesbitt, D. J. Quantum-state resolved reaction dynamics at the gasliquid interface: Direct absorption detection of HF(v,J) product from $F(^2P)$ plus squalane. *J. Chem. Phys.* **2006**, *125*, 021101.
- (3) Ryazanov, M.; Nesbitt, D. J. Quantum-state-resolved studies of aqueous evaporation dynamics: NO ejection from a liquid water microjet. *J. Chem. Phys.* **2019**, *150*, 044201.
- (4) Livingston Large, T. A.; Nesbitt, D. J. Low energy CO scattering at the gas-liquid interface: Experimental/theoretical evidence for a novel sub-thermal impulsive scattering (STIS) channel. *J. Phys. Chem. C* **2020**, *124*, 28006–28017.
- (5) Davidovits, P.; Kolb, C. E.; Williams, L. R.; Jayne, J. T.; Worsnop, D. R. Mass accommodation and chemical reactions at gasliquid interfaces. *Chem. Rev.* **2006**, *106*, 1323–1354.
- (6) Gertner, B. J.; Hynes, J. T. Molecular dynamics simulation of hydrochloric acid ionization at the surface of stratospheric ice. *Science* **1996**, *271*, 1563–1566.
- (7) Ellison, G. B.; Tuck, A. F.; Vaida, V. Atmospheric processing of organic aerosols. J. &eophys. Res. 1999, 104, 11633–11641.
- (8) Sosnowski, T. R.; Kubski, P.; Wojciechowski, K. New experimental model of pulmonary surfactant for biophysical studies. *Colloids Surf.* **2017**, *519*, 27–33.
- (9) King, M. E.; Saecker, M. E.; Nathanson, G. M. The thermal roughening of liquid surfaces and its effect on gas-liquid collisions. *J. Chem. Phys.* **1994**, *101*, 2539–2547.
- (10) Saecker, M. E.; Govoni, S. T.; Kowalski, D. V.; King, M. E.; Nathanson, G. M. Molecular-beam scattering from liquid surfaces. *Science* 1991, 252, 1421–1424.
- (11) Kohler, S. P. K.; Allan, M.; Kelso, H.; Henderson, D. A.; McKendrick, K. G. The effects of surface temperature on the gasliquid interfacial reaction dynamics of $O(^3P)$ + squalane. *J. Chem. Phys.* **2005**, *122*, 024712.
- (12) Wu, B. H.; Zhang, J. M.; Minton, T. K.; McKendrick, K. G.; Slattery, J. M.; Yockel, S.; Schatz, G. C. Scattering dynamics of hyperthermal oxygen atoms on ionic liquid surfaces: [emim][NTf $_2$] and [C $_{12}$ mim][NTf $_2$]. *J. Phys. Chem. C* **2010**, *114*, 4015–4027.
- (13) Faust, J. A.; Nathanson, G. M. Microjets and coated wheels: Versatile tools for exploring collisions and reactions at gas-liquid interfaces. *Chem. Soc. Rev.* **2016**, 45, 3609–3620.
- (14) Lednovich, S. L.; Fenn, J. B. Absolute evaporation rates for some polar and nonpolar liquids. *Am. Inst. Chem. Engin.* **1977**, 23, 454–459.
- (15) King, M. E.; Nathanson, G. M.; Hanninglee, M. A.; Minton, T. K. Probing the microscopic corrugation of liquid surfaces with gasliquid collisions. *Phys. Rev. Lett.* **1993**, *70*, 1026–1029.
- (16) Nathanson, G. M.; Davidovits, P.; Worsnop, D. R.; Kolb, C. E. Dynamics and kinetics at the gas-liquid interface. *J. Phys. Chem.* **1996**, 100, 13007–13020.
- (17) King, M. E.; Fiehrer, K. M.; Nathanson, G. M.; Minton, T. K. Effects of thermal roughening on the angular distributions of trapping and scattering in gas-liquid collisions. *J. Phys. Chem. A* **1997**, *101*, 6556–6561.
- (18) Tesa-Serrate, M. A.; Smoll, E. J.; Minton, T. K.; McKendrick, K. G. Atomic and molecular collisions at liquid surfaces. *Annu. Rev. Phys. Chem.* **2016**, *67*, 515–540.
- (19) Perkins, B. G.; Haber, T.; Nesbitt, D. J. Quantum state-resolved energy transfer dynamics at gas-liquid interfaces: IR laser studies of

- CO_2 scattering from perfluorinated liquids. J. Phys. Chem. B 2005, 109, 16396–16405.
- (20) Perkins, B. G.; Nesbitt, D. J. Quantum-state-resolved CO₂ scattering dynamics at the gas-liquid interface: Incident collision energy and liquid dependence. *J. Phys. Chem. B* **2006**, *110*, 17126–17137.
- (21) Perkins, B. G.; Nesbitt, D. J. Stereodynamics in state-resolved scattering at the gas-liquid interface. *Proc. Natl. Acad. Sci. U.S.A.* **2008**, *105*, 12684–12689.
- (22) Zolot, A. M.; Dagdigian, P. J.; Nesbitt, D. J. Quantum-state resolved reactive scattering at the gas-liquid interface: F + squalane ($c_{30}h_{62}$) dynamics via high-resolution infrared absorption of nascent HF(v,J). *J. Chem. Phys.* **2008**, *129*, 194705.
- (23) Perkins, B. G.; Nesbitt, D. J. Correlated angular and quantum state-resolved CO₂ scattering dynamics at the gas-liquid interface. *J. Phys. Chem. A* **2008**, *112*, 9324–9335.
- (24) Tesa-Serrate, M. A.; King, K. L.; Paterson, G.; Costen, M. L.; McKendrick, K. G. Site and bond-specific dynamics of reactions at the gas-liquid interface. *Phys. Chem. Chem. Phys.* **2014**, *16*, 173–183.
- (25) Allan, M.; Bagot, P. A. J.; Kohler, S. P. K.; Reed, S. K.; Westacott, R. E.; Costen, M. L.; McKendrick, K. G. Dynamics of interfacial reactions between O(³P) atoms and long-chain liquid hydrocarbons. *Phys. Scr.* **2007**, *76*, C42–C47.
- (26) Bagot, P. A. J.; Waring, C.; Costen, M. L.; McKendrick, K. G. Dynamics of inelastic scattering of OH radicals from reactive and inert liquid surfaces. *J. Phys. Chem. C* **2008**, *112*, 10868–10877.
- (27) Perkins, B. G.; Nesbitt, D. J. High resolution dopplerimetry of correlated and quantum state-resolved CO_2 scattering Dynamics at the gas-liquid interface. *Phys. Chem. Chem. Phys.* **2010**, *12*, 14294–14308.
- (28) Lohr, J. R.; Day, B. S.; Morris, J. R. Scattering, accommodation, and trapping of HCl in collisions with a hydroxylated self-assembled monolayer. *J. Phys. Chem. B* **2005**, *109*, 15469–15475.
- (29) Roscioli, J. R.; Bell, D. J.; Nelson, D. J.; Nesbitt, D. J. State-resolved velocity map imaging of surface-scattered molecular flux. *Phys. Chem. Phys.* **2012**, *14*, 4070–4080.
- (30) Roscioli, J. R.; Nesbitt, D. J. Quantum state resolved velocity-map imaging spectroscopy: A new tool for collision dynamics at gas/self-assembled monolayer interfaces. *Far. Discuss.* **2011**, *150*, 471–479.
- (31) Handbook of Chemistry and physics, 52nd ed.; Chemical Rubber Company, 1972.
- (32) Faubel, M.; Schlemmer, S.; Toennies, J. P. A molecular beam study of the evaporation of water from a liquid jet. *Z. Phys. D* **1988**, *10*, 269–277.
- (33) Herriott, D.; Kogelnik, H.; Kompfner, R. Off-axis paths in spherical mirror interferometers. *Appl. Opt.* **1964**, *3*, 523–526.
- (34) Kaur, D.; Desouza, A. M.; Wanna, J.; Hammad, S. A.; Mercorelli, L.; Perry, D. S. Multipass cell for molecular-beam absorption-Spectroscopy. *Appl. Opt.* **1990**, *29*, 119–124.
- (35) Pine, A. S. High-resolution methane ν_3 -band spectra using a stabilized tunable difference-frequency laser system. *J. Opt. Soc. Am.* **1976**, *66*, 97–108.
- (36) Perkins, B. G.; Nesbitt, D. J. Toward three-dimensional quantum state-resolved collision dynamics at the gas-liquid interface: Theoretical investigation of incident angle. *J. Phys. Chem. A* **2009**, *113*, 4613–4625.
- (37) Livingston Large, T. A.; Nesbitt, D. J. Quantum state and doppler-resolved scattering of thermal/hyperthermal DCl at the gasliquid interface: Support for a simple "lever arm" model of the energy-transfer dynamics. *J. Phys. Chem. C* **2019**, *123*, 3449–3460.
- (38) Levine, R. D.; Bernstein, R. B. Molecular Reaction Dynamics and Chemical Reactivity; Oxford University Press: Oxford, 1987.
- (39) Laibinis, P. E.; Whitesides, G. M.; Allara, D. L.; Tao, Y. T.; Parikh, A. N.; Nuzzo, R. G. Comparison of the structures and wetting properties of self-assembled monolayers of normal alkanethiols on the coinage metal surfaces, Cu, Ag, Au. *J. Am. Chem. Soc.* **1991**, *113*, 7152–7167.

- (40) Ulman, A. Formation and structure of self-assembled monolayers. Chem. Rev. 1996, 96, 1533-1554.
- (41) Proch, D.; Trickl, T. A high-intensity multi-purpose piezo-electric pulsed molecular-beam source. *Rev. Sci. Instrum.* **1989**, *60*, 713–716
- (42) Arepalli, S.; Presser, N.; Robie, D.; Gordon, R. J. Detection of Cl atoms and HCl molecules by resonantly enhanced multiphoton ionization. *Chem. Phys. Lett.* **1985**, *118*, 88–92.
- (43) Green, D. S.; Bickel, G. A.; Wallace, S. C. (2 + 1) resonance enhanced multiphoton ionization of hydrogen-chloride in a pulsed supersonic jet spectroscopic survey. *J. Mol. Spectrosc.* **1991**, *150*, 303–353.
- (44) Ashfold, M. N. R.; Nahler, N. H.; Orr-Ewing, A. J.; Vieuxmaire, O. P. J.; Toomes, R. L.; Kitsopoulos, T. N.; Garcia, I. A.; Chestakov, D. A.; Wu, S. M.; Parker, D. H. Imaging the dynamics of gas phase reactions. *Phys. Chem. Chem. Phys.* **2006**, *8*, 26–53.
- (45) Eppink, A. T. J. B.; Parker, D. H. Velocity map imaging of ions and electrons using electrostatic lenses: Application in photoelectron and photofragment ion imaging of molecular oxygen. *Rev. Sci. Instrum.* 1997, 68, 3477–3484.
- (46) Townsend, D.; Minitti, M. P.; Suits, A. G. Direct current slice imaging. *Rev. Sci. Instrum.* **2003**, *74*, 2530–2539.
- (47) Barker, J. A.; Auerbach, D. J. Gas-surface dynamics, velocity distributions, trapping and residence times. *Far. Discuss.* **1985**, *80*, 277–289.
- (48) Ziemkiewicz, M. P.; Roscioli, J. R.; Nesbitt, D. J. State-to-state dynamics at the gas-liquid metal interface: Rotationally and electronically inelastic scattering of $NO[^2\Pi_{1/2}(0.5)]$ from molten gallium. *J. Chem. Phys.* **2011**, *134*, 234703.
- (49) Lancaster, D. K.; Johnson, A. M.; Kappes, K.; Nathanson, G. M. Probing gas—liquid interfacial dynamics by helium evaporation from hydrocarbon liquids and jet fuels. *J. Phys. Chem. C* **2015**, *119*, 14613—14623.
- (50) Wilson, K. R.; Rude, B. S.; Catalano, T.; Schaller, R. D.; Tobin, J. G.; Co, D. T.; Saykally, R. J. X-ray Spectroscopy of liquid water microjets. *J. Phys. Chem. B* **2001**, *105*, 3346–3349.
- (51) Williams, H. L.; Erickson, B. A.; Neumark, D. M. Time-resolved photoelectron spectroscopy of adenosine and adenosine monophosphate photodeactivation dynamics in water microjets. *J. Chem. Phys.* **2018**, *148*, 194303.
- (52) Faubel, M.; Kisters, T. Non-equilibrium molecular evaporation of carboxylic acid dimers. *Nature* **1989**, 339, 527–529.
- (53) Hahn, C.; Kann, Z. R.; Faust, J. A.; Skinner, J. L.; Nathanson, G. M. Super-maxwellian helium evaporation from pure and salty water. *J. Chem. Phys.* **2016**, *144*, 044707.
- (54) Miksch, G.; Weber, H. G. Laser diagnostics of surface-emitted na₂ molecules. *Chem. Phys. Lett.* **1982**, 87, 544–547.
- (55) Maselli, O. J.; Gascooke, J. R.; Lawrance, W. D.; Buntine, M. A. Benzene internal energy distributions following spontaneous evaporation from a water-ethanol solution. *J. Phys. Chem. C* **2009**, *113*, 637–643.
- (56) Barinkova, V. Photoejection of molecules from the surface of a liquid microjet. Ph.D. Thesis, University of Leicester, 2009.
- (57) Ziemkiewicz, M. P.; Zutz, A.; Nesbitt, D. J. Inelastic scattering of radicals at the gas-ionic liquid interface: Probing surface dynamics of bmim-Cl, bmim-BF₄, and bmim-Tf₂N by rovibronic scattering of NO[${}^{2}\Pi_{1/2}(0.5)$]. *J. Phys. Chem. C* **2012**, *116*, 14284–14294.
- (58) Zutz, A.; Nesbitt, D. J. Nonadiabatic spin—orbit excitation dynamics in quantum-state-resolved NO($^2\Pi_{1/2}$) scattering at the gas—room temperature ionic liquid interface. *J. Phys. Chem. C* **2015**, *119*, 8596–8607.
- (59) Zutz, A.; Nesbitt, D. J. Quantum state-resolved molecular scattering of $NO(^2\Pi_{1/2})$ at the gas- c_n -mim Tf_2N room temperature ionic liquid interface: Dependence on alkyl chain length, collision energy, and temperature. *Am. Inst. Phys. Adv.* **2016**, *6*, 105207.
- (60) Zutz, A.; Nesbitt, D. J. Angle-resolved molecular beam scattering of NO at the gas-liquid interface. *J. Chem. Phys.* **2017**, 147, 054704.

Accounts of Chemical Research

- (61) Zutz, A.; Nesbitt, D. J. Quantum-state-resolved scattering of $NO(^2\Pi_{1/2})$ from hot molten Au(liq): On the role of thermal electronhole pairs in vibrational excitation dynamics. *J. Phys. Chem. C* **2018**, 122, 17161–17169.
- (62) Rayleigh, L. On the instability of jets. *Proc. London Math. Soc.* 1878, s1-10, 4-13.
- (63) Luque, J.; Crosley, D. R. Lifbase: Database and spectral simulation program (version 1.6); HITRAN: 1999.
- (64) Atomic and molecular beam methods; Oxford University Press, 1988.
- (65) Snow, W. R.; Dowell, J. T.; Chevrenak, J. G.; Berek, H. E. Molecular beam measurements of total collision cross sections of H₂O. *J. Chem. Phys.* **1973**, *58*, 2517–2520.
- (66) Cappelletti, D.; Candori, P.; Roncaratti, L. F.; Pirani, F. A molecular beam scattering study of the weakly bound complexes of water and hydrogen sulphide with the main components of air. *Mol. Phys.* **2010**, *108*, 2179–2185.